

See discussions, stats, and author profiles for this publication at: <https://www.researchgate.net/publication/231654376>

Enhanced Electron Transport in Dye-Sensitized Solar Cells Using Short ZnO Nanotips on A Rough Metal Anode

ARTICLE *in* MRS ONLINE PROCEEDING LIBRARY · NOVEMBER 2009

DOI: 10.1021/jp908678x

CITATIONS

51

READS

69

5 AUTHORS, INCLUDING:



[Yasuo Ito](#)

Northern Illinois University

26 PUBLICATIONS 869 CITATIONS

[SEE PROFILE](#)



[Wai-Kwong Kwok](#)

Argonne National Laboratory

534 PUBLICATIONS 14,132 CITATIONS

[SEE PROFILE](#)

Enhanced Electron Transport in Dye-Sensitized Solar Cells Using Short ZnO Nanotips on A Rough Metal Anode

Zhenzhen Yang,[†] Tao Xu,^{*,†} Yasuo Ito,[‡] Ulrich Welp,[§] and Wai Kwong Kwok[§]

Department of Chemistry and Biochemistry, Northern Illinois University, DeKalb, Illinois 60115, Department of Physics, Northern Illinois University, DeKalb, Illinois 60115, and Materials Science Division, Argonne National Laboratory, Argonne, Illinois 60439

Received: September 8, 2009; Revised Manuscript Received: October 7, 2009

Many efforts have been directed toward the enhancement of electron transport in dye-sensitized solar cells (DSSC) using one-dimensional nanoarchitected semiconductors. However, the improvement resulting from these ordered 1-D nanostructured electrodes is often offset or diminished by the deterioration in other device parameters intrinsically associated with the use of these 1-D nanostrucutres, such as the two-sided effect of the length of the nanowires impacting the series resistance and roughness factor. In this work, we mitigate this problem by allocating part of the roughness factor to the collecting anode instead of imparting all the roughness factors onto the semiconductor layer attached to the anode. A microscopically rough Zn microtip array is used as an electron-collecting anode on which ZnO nanotips are grown to serve as the semiconductor component of the DSSC. For the same surface roughness factor, our Zn-microtip|ZnO-nanotip DSSC exhibits an enhanced fill factor compared with DSSCs that have ZnO nanowires supported by a planar anode. In addition, the open-circuit voltage of the Zn-microtip|ZnO-nanotip DSSC is also improved due to a favorable band shift at the Zn–ZnO interface, which raises the Fermi level of the semiconductor and consequently enlarges the energy gap between the quasi-Fermi level of ZnO and the redox species. With these improvements, the overall efficiency becomes 1.4% with an open-circuit voltage of 770 mV, while the surface roughness factor of ZnO is approximately 60. Electrochemical impedance spectroscopic study reveals that the electron collection time is much shorter than the electron lifetime, suggesting that fast electron collection occurs in our device due to the significantly reduced electron collection distance along the short ZnO nanotips. The overall improvement demonstrates a new approach to enhance the efficiency of dye-sensitized solar cells.

Introduction

As the global climate change becomes more and more evident with each passing decade, cutting greenhouse gas emissions from energy production must be our top priority in order to minimize future climate changes. The large abundance of solar energy promises to be the most reliable clean energy source. Effective utilization of solar energy relies on the development of efficient photovoltaic devices, among which dye sensitized solar cells (DSSCs) have drawn much attention due to their low cost and simple fabrication procedures. The most extensively studied DSSCs are based on an n-type semiconducting TiO₂ nanoparticulate film that harvests the electrons from the lowest unoccupied molecular orbitals (LUMO) of photoexcited dyes to the conduction band of the semiconductors and transports the electrons to the collecting anode.^{1,2} Concurrently, the oxidized dyes are reduced by redox species that convey electrons from the counter electrode. However, the record high conversion efficiency of DSSCs (11.2%) has remained unchanged for nearly two decades.³ Therefore, more basic research effort is needed to alter the structure and/or the nature of the components in the DSSCs, particularly in the semiconducting layer that bridges the dyes and the electron collecting anode, in order to optimize the electron-transfer energetics and kinetics. For example, enhanced electron transfers were reported in various n-type

semiconducting layers consisting of arrays of one-dimensional (1-D) nanostructures, including ZnO nanowires and nanotubes,^{4–9} TiO₂ nanowires and nanotubes,^{10–14} etc. These highly ordered 1-D semiconducting nanostructures provide an ordered pathway for electrons percolating to the collecting anode, in contrast to the highly disordered electron pathway found in a nanoparticulate layer that can lead to significant scattering of free electrons at the particle–particle interfaces.^{4,9,15} In addition, if the radius of the 1-D n-type semiconductors is large enough, an upward band bending at the semiconductor surface can form, which suppresses the adverse back electron transfers (charge recombination) from the semiconductor to the electrolyte or to the oxidized dyes.^{9,16} This is because the Fermi level of an n-type semiconductor is typically higher than the redox potential of the electrolyte. To equilibrate the two electron levels, electrons flow from the semiconductor into the electrolyte. As a result, there is a built-in circular electric field from the surface of the semiconductor nanowires toward their centers. This internal electric field pulls the injected electron toward the center of the wire and reduces the interception of the electrons by the electrolyte around the surface of the wire. The suppression of back electron transfer improves the current density of the cells.

However, so far, none of these ordered 1-D semiconductor-based DSSCs have achieved an efficiency that exceeds that of a conventional TiO₂ nanoparticle-based DSSC. This is because many other device parameters are often interlinked, which can offset or reduce the improvements brought by the new features. A particular problem reported by Yang and co-workers is the

* To whom correspondence should be addressed. E-mail: txu@niu.edu.

[†] Department of Chemistry and Biochemistry, Northern Illinois University.

[‡] Department of Physics, Northern Illinois University.

[§] Argonne National Laboratory.

diametric opposing effect resulting from increasing the length of the ZnO nanowires.⁹ On one hand, longer wires exhibit higher short-circuit current (J_{sc}) due to the increased surface area and thus higher dye loading. On the other hand, longer wires lead to higher series resistance, thus lowering the fill factor (FF).⁸ Narrower, thus denser, nanowires appear as a potential approach to overcome this problem. However, if the Debye–Hückel screening length exceeds the wire radius, reducing the diameter of the wires can eliminate the upward band bending at the wire's surface,^{8,9} an advantage of 1-D semiconductors explained above. Typically, depending on the carrier density and the electrolyte, the width of the depletion layer can extend to tens of nanometers into the ZnO wires.¹⁶ These dilemmas make it especially desirable to explore further innovations in 1-D ordered semiconductor-based DSSCs that can provide new basic science to improve this fascinating photovoltaic device.

In this paper, we aim to retain the state-of-the-art strategy of enhancing the electron transfer afforded in ordered 1-D semiconductor structures but simultaneously plan to reduce the series resistance of the semiconductor without a significant loss of surface roughness compared to 1-D nanowires. Rather than placing all the roughness onto the semiconductor layer, our strategy is to allocate part of the roughness onto the collecting anode. A rough collecting anode provides a larger surface area to accommodate more individual 1-D nanoscale semiconductors. Hence, for the same level of surface roughness factor (SRF, defined as the ratio of the total semiconductor surface area to the nominal planar substrate area),⁹ the length of the 1-D semiconductor on a coarsened anode can be relatively shorter than that of conventional 1-D semiconductors supported on a planar anode. We demonstrate this strategy by employing a Zn-microtip|ZnO-nanotip core–shell hierarchical nanoarchitecture as the anode semiconductor component in the DSSC. The realigned band structure at the metal–semiconductor interface affects the Fermi level of the semiconductor¹⁷ and provides us with a potential opportunity to improve the open-circuit voltage of the cells, a key parameter governing the attainable power from a DSSC.

Experimental Methods

Preparation of Anode Semiconductor Component. The fabrication of the Zn-microtip|ZnO-nanotip core–shell hierarchy nanoarchitecture follows the method reported by Leu et al.^{18,19} A zinc foil (99.99%, Alfa Aesar) was first mechanically polished to a good mirrored surface, followed by a subsequent electropolishing in a solution composed of absolute ethanol and 85% phosphoric acid (2:1 v/v) for 5 min at a current density of 70 mA/cm² (calculation includes both sides of the foil) under 3 °C. A highly ordered array of Zn microtips can be obtained by anodizing the polished Zn foil in a freshly prepared NH₄Cl/H₂O₂ (32:1 M/M) aqueous solution for 60 s at a current density of 14 mA/cm². After the anodization, the Zn foil was dipped into a ZnO growth solution prepared by combining a 0.5 M Zn(NO₃)₂ solution and a 4.0 M KOH solution (1:1 v/v). After 30 min, ZnO nanotips formed on the Zn microtips. We observed the growth of 300 nm long ZnO nanotips on the surface of the Zn microtips. The resulting Zn-microtip|ZnO-nanotip was heated in ozone at 150 °C for 20 min to passivate the exposed Zn metals with a thin ZnO layer.

Dye Sensitizing. Unlike the dye sensitization process for TiO₂ nanoparticles, in which the TiO₂ film is inert and can be impregnated in the acidic dye solution for days, the sensitization of the Zn-microtip|ZnO-nanotip electrode was carried out in a 0.3 mM [RuL2(NCS)2]:2 TBA (L = 2,2'-bipyridyl-4,4'-dicarboxylic acid, TBA = tetra-*n*-butylammonium (N719 dye,

Dyesol, Australia) solution for only 2 h using aprotic acetonitrile as solvent for the best performance.²⁰ This is because one needs to avoid the dissolution of ZnO in the acidic N719 dye solution and the consequent formation of the Zn²⁺/dye complexes, which can diminish the light absorption.^{20–22}

Preparation of Platinized Counter Electrode. Platinized counter electrodes were fabricated by thermally coating an ultrathin Pt layer onto a piece of FTO (fluorinated SnO₂, Solaronix, Switzerland) glass in an evaporator (Edwards 306 A) at a rate of 1 Å/s). The nominal thickness of the Pt film was measured to be 2 nm using a quartz crystal thickness monitor.

Solar Cell Fabrication. The dye-sensitized solar cell was assembled by sandwiching the dye-sensitized Zn-microtip|ZnO-nanotip anode semiconductor component with the Pt-coated FTO cathode using a piece of hot melt Surlyn (25 μm thick, Solaronix) as a spacer. The internal space of the cell was filled with an electrolyte (0.5 M LiI, 50 mM I₂, 0.5 M 4-*tert*-butylpyridine in 3-methoxypropionitrile) by capillary force through a small predrilled hole in the counter electrode. The total active electrode area was 0.50 cm².

Structure Characterization. The Zn-microtip|ZnO-nanotip electrode was characterized using a TeScan (model Vega II SBH) tungsten filament scanning electron microscope (SEM) and a JEOL JSM 2010 transmission electron microscope (TEM).

Device Characterization. The current density–voltage (J – V) curves were collected using a potentiostat (Gamry Reference 600) at 1 sun 1.5 air mass global (AM G) spectrum provided by a solar simulator (Photo Emission Inc., CA, model SS50B).

The Gamry Reference 600 potentiostat was equipped with an EIS300 software to conduct the electrochemical impedance spectroscopy (EIS) study, which is used to determine the electron-transport performance of the solar cell. For EIS measurements, a sandwiched cell was used in a two-electrode configuration under dark condition. The EIS spectra were obtained at forward bias potentials in a frequency range from 0.06 to 60 kHz with an ac amplitude of 10 mV. The Z-view modeling program was used to model and fit the spectra data by inserting a built-in extended element (DX type11-Bisquert #2) in the equivalent circuit, which allows for transmission line modeling.

The measurement of the dye-loading amount was conducted by soaking an N-719 sensitized sample (area = 0.5 cm²) in 3 mL of 10 mM KOH for 2 h (target solution). The UV–vis spectra of the target solution and three solutions with known dye concentrations (calibration solutions) were measured. On the basis of Beer's law, the concentration of the target solution can be obtained by fitting the absorbance at 522 nm (with respect to blank solvent) to the calibration curve.

Results and Discussion

Device Structure. Figure 1 shows the high- (a) and low-magnification (b) SEM images of the nearly circular cone-shaped Zn microtips after anodization for 60 s. The average height and base radius of the cone-shaped Zn microtips were measured to be approximately 3 μm (h) and 0.6 μm (r), respectively, while the average packing density was measured to be ~2.5 tips/μm². Given the lateral area for a cone of $\pi r(h^2 + r^2)^{1/2}$, the geometry parameters yield an SRF of ~12 for this microscopically coarsened Zn foil.

This coarsened Zn foil is then used as the collecting anode on which cone-shaped ZnO nanotips of different lengths were self-assembled to form the Zn-microtip|ZnO-nanotip core–shell hierarchical nanoarchitecture. Figure 2a illustrates a typical large area (50 μm × 50 μm) SEM image of the nanostructure. The top-view (Figure 2b) and side-view (Figure 2c) images of an

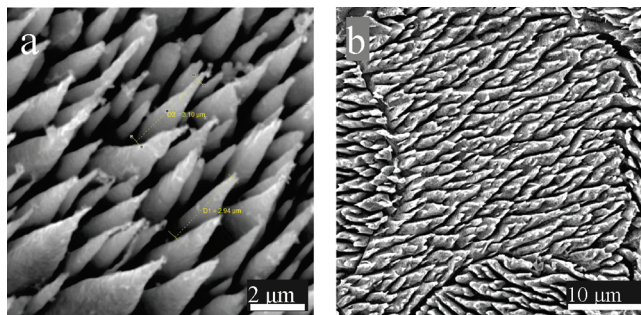


Figure 1. (a) High-magnification SEM image of a Zn microtip array formed by anodization of a Zn foil. (b) SEM image of a large area ($40 \mu\text{m} \times 40 \mu\text{m}$).

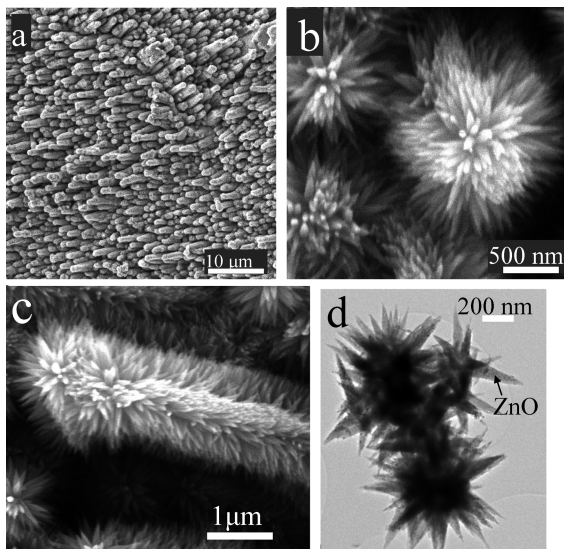


Figure 2. (a) Representative large area SEM image of Zn nanotips grown on an array of Zn microtips. (b) A magnified SEM top-view image of Zn nanotips grown on Zn microtips. (c) A magnified SEM top-view image of the Zn nanotips grown on the Zn microtips. (d) A TEM image of the apex of the Zn-microtip/ZnO-nanotip core–shell hierarchy nanoarchitecture.

individual pinecone-like Zn-microtip/ZnO-nanotip structure show that the ZnO nanotips are densely packed. The apex part of the pinecone is thin enough for TEM study. Figure 2d shows the TEM image of the apex part of the pinecone and demonstrates that the Zn cores are surrounded by ZnO nanotips. Both SEM and TEM images clearly illustrate that the average length of the ZnO nanotips is approximately 300 nm and the base radius is approximately 50 nm. We counted approximately 600 ZnO nanotips on each Zn microtip. The average lateral area of each ZnO nanotip is calculated to be $\sim 0.05 \mu\text{m}^2$. Thus, we estimate the SRF of our Zn-microtip/ZnO-nanotip electrode to be ~ 60 . Compared to reported ZnO nanowires, this SRF is equivalent to an array of 100 nm diameter ZnO nanowires that are $6 \mu\text{m}$ in length and $\sim 35 \text{ wires}/\mu\text{m}^2$ in wire packing density. For reference, the reported packing density of ZnO nanowires with a diameter of 100 nm ranges between 28 and 40.^{5–8,23} The possible exposed Zn metal is treated by ozone to enhance the shunt resistance.

Figure 3 illustrates the structure of a DSSC using the above Zn-microtip/ZnO-nanotip plate as the anode semiconductor component. The device is illuminated from the cathode side, in the same fashion as that of many other 1-D semiconducting nanoarchitecture-based DSSCs.^{13,24–26}

Device Performance. Figure 4 is the J – V characteristics of such a DSSC under 1 sun (AM 1.5 G) illumination. The crucial

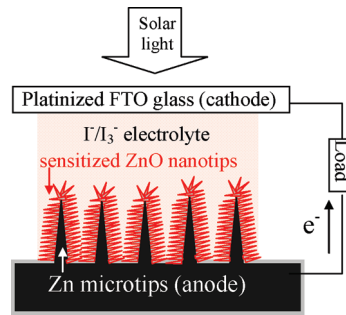


Figure 3. Schematic diagram of the DSSC based on a Zn-microtip/ZnO-nanotip core–shell hierarchy nanoarchitected electrode (note that the drawing is not to scale).

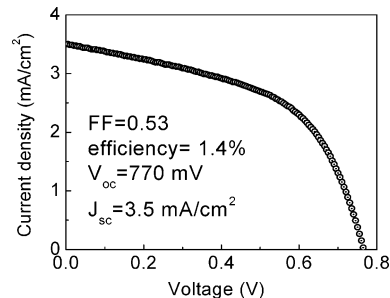


Figure 4. Representative current density–voltage (J – V) curve of the DSSC using Zn-microtip/ZnO-nanotip as the anode semiconductor component.

parameters are summarized in Table 1, along with the reported values for other DSSCs that are based on a planar anode-supported ZnO nanowire design.^{5–9} For comparison, we list the SRFs of all cells that are either mentioned in the literature or calculated by us based on the length, diameter, and wire density obtained from their published SEM images.

The measured J_{sc} for our Zn-microtip/ZnO-nanotip nanoarchitecture-based DSSCs is $3.5 \text{ mA}/\mu\text{m}^2$. This value is close to that of the planar anode-supported ZnO nanowires with the same SRF, which indicates that the dye-loading amount ($1.1 \times 10^{-8} \text{ mol}/\text{cm}^2$) of our device is comparable with that of ZnO nanowires possessing the same SRF.⁹ Branched ZnO nanowires exhibit an improved photocurrent because of the increased surface area, thus an increased dye-loading amount. Other ZnO hierarchical nanostructures also show enhanced photocurrent due to increased surface area.²⁷ In fact, the J_{sc} of our device is underestimated because the incident light is diminished by the Pt layer on the counter electrode, as observed in its transmittance in comparison to a bare FTO glass (Figure 5). Nonetheless, two key parameters of our device, the fill factor (FF) and open-circuit voltage (V_{oc}), show pronounced improvements over DSSCs based on planar anode-supported ZnO nanowires.

The fill factors previously reported for DSSCs based on planar anode-supported ZnO nanowires are typically between 0.3 and 0.4.^{5–9} In contrast, the fill factor of our device is consistently greater than 0.5. This trend agrees with the reported enhancement of the fill factor through the reduction of the series resistance in ZnO nanowires using interconnected ZnO nanowires.⁷ For the same roughness factor (SRF = 60), the series resistance of our ZnO nanotips is greatly reduced due to the much shorter tip length ($\sim 0.3 \mu\text{m}$) compared with the planar-supported ZnO nanowires ($6–7 \mu\text{m}$). This 20-fold reduction in the length of our ZnO nanotips results in a series resistance $R_s = dV/dJ_{(J=0)}$ as low as $28 \Omega \text{ cm}^2$. For the same SRF, this R_s value is significantly lower than that of DSSCs based on planar anode-supported ZnO nanowires, ranging between 46 and 106

TABLE 1: Comparison of Cell Parameters between Our Zn-Microtip/ZnO-Nanotip DSSCs (Averaged from Four Samples) and 1-D ZnO-Nanowire (NW)-Based DSSCs Reported in the Literature^a

	SRF ^b	J_{sc} (mA/cm ²)	V_{oc} (mV)	FF	η (%) ^c
ZnO nanotips on rough Zn	60	3.6 ± 0.4	760 ± 22	0.53 ± 0.02	1.4 ± 0.1
ZnO NWs on planar FTO anode ⁹	75, 200	2.5, 6	650	0.4, 0.37	0.8, 1.5
ZnO NWs on planar FTO anode ⁶	30	2.0	660–680	0.4	0.55
ZnO NWs on planar FTO anode ⁵	120	4.5	630	0.36	1.0
ZnO NWs on planar FTO anode ⁷	60	2.4	630	0.49	0.75
ZnO NWs on planar FTO anode ⁸	60	4	600	0.32	0.77
branched ZnO NWs on planar FTO ⁵	>>120	5	650	0.55	1.9
branched ZnO NWs on planar FTO ⁷	>>60	4.3	670	0.52	1.51
hierarchical ZnO on planar FTO ²⁷	>>60	4.4	442	0.37	0.74

^a The dye used in all DSSCs is N719. ^b The surface roughness factors (SRFs) are estimated based on the SEM images of published reports.

^c The device efficiency (η) is given by $\eta = J_{sc} \times V_{oc} \times FF / (100 \text{ mW/cm}^2)$.

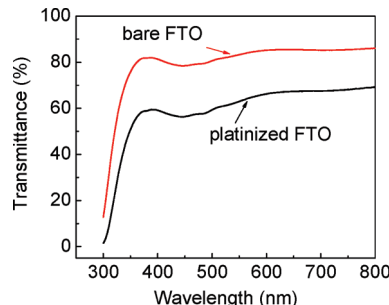


Figure 5. UV-vis transmittance of a platinized FTO glass and a bare FTO glass.

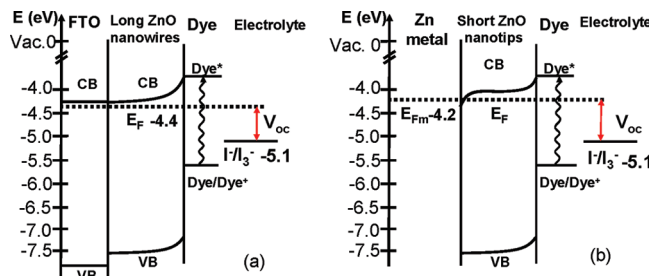


Figure 6. Highly idealized energy diagrams of DSSCs using (a) planar FTO-supported long ZnO nanowires as the anodeselector component. (b) Zn-microtip/ZnO-nanotip as the anodeselector component.

$\Omega \text{ cm}^2$.^{7,8} Therefore, we attribute the enhanced fill factor found in our device to the reduced series resistance in the shorter ZnO nanotips.

The V_{oc} 's of our Zn-microtip/ZnO-nanotip DSSCs were measured to be consistently about 770 mV, greater than reported values for long ZnO nanowire-based DSSCs that are typically below 700 mV, as summarized in Table 1. The maximum value of V_{oc} is determined by the energy gap between the quasi-Fermi level in ZnO under illumination and the redox potential of the I/I_3^- electrolyte.²⁸ The enhancement in V_{oc} of our Zn-microtip/ZnO-nanotip DSSC can be elucidated by comparing its energy diagram with that of a planar-supported ZnO nanowire DSSC. Figure 6a is the highly idealized energy diagram of a planar FTO anode-supported ZnO nanowire-based DSSC. The upward band bending at the ZnO–electrolyte interface is due to the higher Fermi level of n-type ZnO compared to the redox potential of the electrolyte, and hence, electrons will flow from the electrode into the electrolyte until equilibrium is established.¹⁶ Consequently, there is a positive space charge region in the center of the wires, which is reflected as the upward bending at the wire surface. This electron depletion layer in ZnO nanowires can extend into the semiconductor over a few

nanometers to a few tens of nanometers, depending on the carrier density and the dielectric constant of the semiconductor, as well as the electrolyte. For example, even at a fairly high carrier density of $10^{18}/\text{cm}^3$, the diameter of a ZnO nanowire should at least be 20 nm to attain a potential drop of 0.2 V across the depletion layer in a carbonate propylene electrolyte (0.1 M LiClO₄).¹⁶

Figure 6b is the energy diagram of the DSSC using our Zn-microtip/ZnO-nanotip core–shell nanoarchitecture as the anodeselector component. Considering the fact that a large portion of a ZnO nanotip has a radius above 20 nm, an upward band bending should also exist at the ZnO-nanotip–electrolyte interface in our device, similar to the case of planar anode-supported ZnO nanowires. Besides, an added feature in our device is a metal/n-type semiconductor Ohmic junction established at the interface between Zn and ZnO nanotips. This is because the Fermi level of Zn (-4.2 eV)^{29,30} is higher than that of ZnO (-4.4 eV , average value reported as the Fermi level for ZnO).^{31–34} To achieve thermal equilibrium in this junction, electrons must flow from the Zn metal into the lower-energy states of the conduction band in the n-type semiconductor, that is, ZnO, which makes the ZnO in the junction region more n-type.¹⁷ As a consequence, we believe that the Fermi level of the entire ZnO nanotip is raised because the length of our ZnO nanotips is so short that a considerable section of the wire is affected by the electron accumulation layer. The width of the junction (w) can be estimated using $w = \sqrt{2\varepsilon_0\varepsilon_r V_b/(eN_d)}$,³⁵ where ε_0 is the vacuum permittivity; $\varepsilon_r = 10$ is the dielectric constant of ZnO nanowires;¹⁶ V_b is the amount of band bending, assumed to be 0.2 V; e is the elementary charge; N_d is the carrier density of ZnO; and we assume $N_d = 10^{17} \text{ cm}^{-3}$. Thus, w is estimated to be approximately 50 nm. As a result, the V_{oc} , that is, the energy gap between the quasi-Fermi level of ZnO and the electrolyte redox potential, is widened, which takes into account a band-edge upshift of ZnO of about 0.15 eV due to the accumulation of electrons from the Zn metal. In contrast, if there is an electron accumulation layer at the interface between the much longer ZnO nanowires and the planar FTO anode, it can only affect a relatively small portion (at the root of the nanowires) of the entire nanowires. Therefore, this effect is not considered in Figure 6a for long ZnO nanowires on FTO.

Kieven et al. reported that the shorter the ZnO nanowires, the better the photovoltage, because the shorter electron collection distance suffers less from the competing kinetic process, namely, the charge recombination process.³⁶ Therefore, the enhanced open-circuit voltage in our device can also be contributed from the fact that the short ZnO nanotips provide a short electron collection distance to the metal Zn. Such a short

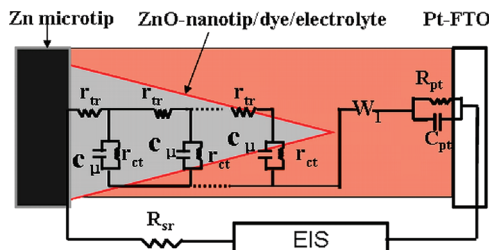


Figure 7. The equivalent circuit model to which impedance spectra are fit, where r_{tr} is the transport resistance of the electrons in the ZnO, r_{ct} is the charge-transfer resistance of the charge recombination between electrons in the ZnO and redox shuttle in the electrolyte, C_μ is the chemical capacitance, R_{sr} is a lumped series resistance for the transport resistance of Zn and all resistances out of the cell, W_1 is the impedance of diffusion of the redox species in the electrolyte, and R_{pt} and C_{pt} are the charge-transfer resistance and interfacial capacitance at the Pt-FTO/electrolyte interface, respectively.

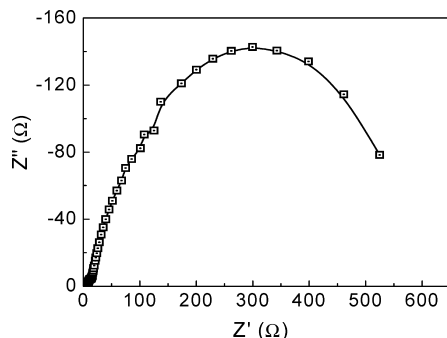


Figure 8. Representative Nyquist plot of the impedance data of the Zn/ZnO core–shell nanotip DSSC at 450 mV forward bias in the dark.

collection distance makes charge transport much more competing than the charge recombination process. Thus, we further studied the kinetics of electron collection time and electron lifetime.

Electrochemical Impedance Spectroscopy. Electrochemical impedance spectroscopy is an effective technique for elucidating the competition between the electron interception (typically by I_3^-) and the electron diffusion to the collecting anode (herein, the Zn metal). As a useful point of reference, the most efficient (i.e., 10–11% power efficiency) DSSCs to date have been characterized using EIS.³⁷ Similar to this and other reports,^{38–40} a geometrically appropriate equivalent circuit of our DSSCs, which contains three interfaces formed by Zn/ZnO, ZnO/dye/electrolyte, and electrolyte/Pt-FTO, is illustrated in Figure 7. Because the possible exposed Zn metal is passivated in ozone, the communication of electrolyte with Zn metal is not considered here. In Figure 7, R_{sr} is a lumped series resistance for the transport resistance of Zn and all resistances out of the cell; R_{pt} and C_{pt} are the charge-transfer resistance and interfacial capacitance at the platinized-FTO/electrolyte interface, respectively; W_1 is the impedance of diffusion of the redox species in the electrolyte; C_μ is the chemical capacitance, accounting for the energy storage by virtue of carrier injection; r_{tr} is the microscopic electron diffusion resistance, which reflects the charge-transport resistance in ZnO nanotips; and r_{ct} is the microscopic charge-transfer resistance, indicating the resistance against the charge recombination events from the phase of high to the phase of low Fermi level.

A representative Nyquist plot, Figure 8, shows the characteristic impedance features of a Zn-microtip/ZnO-nanotip DSSC at 450 mV forward bias (defined as when the Zn electrode is negatively biased and the counter platinized FTO electrode is positively biased). The impedance spectra at all voltages are

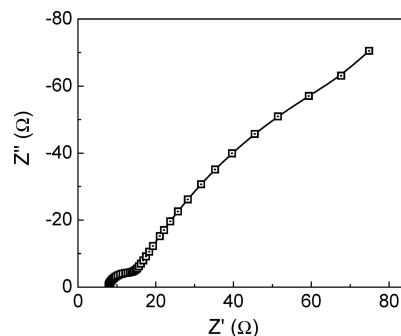


Figure 9. 10 \times magnified panel of the same spectrum in Figure 7 to highlight the high-frequency response.

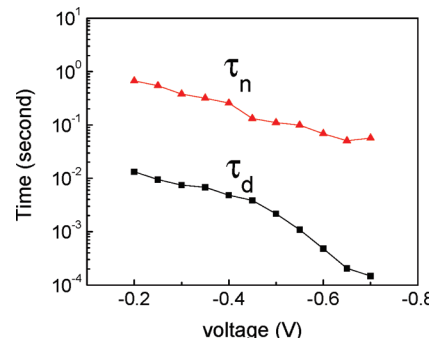


Figure 10. Charge lifetime (triangle) and charge collection time (squares) as a function of applied voltage for the Zn-microtip/ZnO-nanotip core–shell architecture-based DSSC.

fitted based on the suggested equivalent circuit according to Bisquert's diffusion-recombination model.³⁷ Good fits to the equivalent circuit model were obtained at all applied potentials investigated. Estimated parameters of the electron transport in the device were extracted from the Nyquist plots according to the procedure proposed by Adachi et al.³⁷ The low-frequency semicircle in Figure 8 is assigned to the macroscopic charge-transfer resistance, R_{ct} related to the macroscopic recombination of electrons ($R_{ct} = r_{ct}/L$) at the ZnO/electrolyte interface,³⁵ where L is the thickness of the semiconductor, that is, the length of the ZnO tip. The very small semicircle magnified in Figure 9 is assigned to the resistance of Pt and capacitance C_{pt} of the electrolyte/Pt cathode interface. In addition, the short section along the straight line of $Z'' = Z'$ at high frequency reflects the macroscopic electron-transport resistance R_{tr} ($R_{tr} = r_{tr}L$) in ZnO.³⁵ From Figure 9, it is clear that the charge recombination process is 2–3 orders of magnitude slower than the diffusion through the ZnO layer in this case ($R_{ct} \gg R_{tr}$).

It is more convenient to discuss the electron collection efficiency in terms of the characteristic electron-transport time (τ_d) and electron lifetime (τ_n), because these time constants can also be obtained using alternative techniques, such as time transients of intensity modulated photocurrent spectroscopy (IMPS).^{41,42} If the capacitance C_μ is taken to be strictly “chemical” in nature (reflecting density of states), it is rational to assume a multiple trapping diffusion interpretation in which $\tau_d = R_{tr}C_\mu$ and $\tau_n = R_{ct}C_\mu$.⁴³ Figure 10 is the comparison in charge collection time (τ_d , squares) and charge lifetime (τ_n , triangles) for the Zn/ZnO nanotip DSSC. Several features of the Zn-microtip/ZnO-nanotip DSSC charge dynamics are noteworthy in Figure 10. First, a roughly linear and parallel trend in τ_d and τ_n with increasing applied potential is observed, in agreement with the results reported by Martinson et al.⁴³ Furthermore, τ_d is 2–3 orders of magnitude faster than τ_n at all measured potentials. This is also indicated in Figure 8 as $R_{tr} \ll R_{ct}$. The much faster electron collection process compared with

the electron lifetime is attributed to the significantly reduced collection distance, namely, the length of the ZnO tips in our Zn/ZnO core–shell structure in comparison with the planar-supported ZnO nanowires with the same SRF. The faster electron collection helps the accumulation of electrons in the conduction band of ZnO, leading to the rise of electron density (chemical potential) of the ZnO, thus increasing V_{oc} . Meanwhile, the faster electron collection limits the back electron transfer. Hence, more electrons can reach the collecting electrode, which results in an enhanced J_{sc} in our device in comparison with the J_{sc} found in long ZnO nanowires on planar the anode, as indicated in Table 1.

Conclusions

In summary, we have demonstrated that a microscopically rough Zn foil can be used as a collecting anode in a DSSC to accommodate more 1-D ZnO semiconducting nanostructures than a planar anode. In this way, the interlink between the length and the surface roughness of the 1-D nanostructured anode can be somewhat decoupled. For the same surface roughness factor of the semiconducting layer, the length of the ZnO nanotips supported on such a rough Zn anode can be much shorter than that of the ZnO nanowires supported on a planar anode. As a result, the Zn-microtip/ZnO-nanotip DSSC exhibits an enhanced fill factor compared with the longer ZnO nanowires-based DSSC due to the reduced series resistance in shorter ZnO nanotips. In addition, shorter ZnO nanotips lead to a shorter electron collection distance and faster (2–3 orders of magnitude) electron collection time than the electron lifetime, which acts to suppress electron interception (charge recombination) by the electrolyte and hence improves the current density of the device. Moreover, the open-circuit voltage is also increased in the Zn-microtip/ZnO-nanotip DSSC because the electron accumulation layer at the Zn/ZnO interface affects a considerable portion of the short ZnO nanotips, thus raising the Fermi level of the entire ZnO nanotips. By allocating part of the roughness factor to the collecting anode instead of imparting all the roughness factors onto the semiconductor layer attached to the anode, our design exhibits an advantage over the branched ZnO; that is, the electron collection distance in the semiconductor layer can be significantly shortened. Thus, the forward electron transport suffers less from back electron transfer. This strategy presented here provides an alternative fundamental strategy for enhancing the open-circuit voltage in DSSCs. Certainly, in contrast to the surface roughness factor of a TiO₂ nanoparticulate film, typically well above 1000, the surface roughness factor of our Zn-microtip/ZnO-nanotip electrode is still very low. However, it is possible to improve the roughness in the metal anode by lithographic methods, which is capable of making taller and denser metal tips.

Acknowledgment. We acknowledge the financial support from the American Chemical Society Petroleum Research Fund (Type G 46374-G10) and the U.S. Department of Energy, under contract No. DE-AC02-06CH11357. T.X. is grateful for the stimulating discussions with Dr. Alex B. F. Martinson at the Materials Science Division, Argonne National Laboratory.

References and Notes

- O'Regan, B.; Grätzel, M. *Nature* **1991**, *353*, 737–740.
- Grätzel, M. *Nature* **2003**, *421*, 586–587.
- Nazeeruddin, M. K.; De Angelis, F.; Fantacci, S.; Selloni, A.; Viscardi, G.; Liska, P.; Ito, S.; Takeru, B.; Grätzel, M. G. *J. Am. Chem. Soc.* **2005**, *127*, 16835–16847.
- Martinson, A. B. F.; Elam, J. W.; Hupp, J. T.; Pellin, M. J. *Nano Lett.* **2007**, *7*, 2183–2187.
- Jiang, C. Y.; Sun, X. W.; Lo, G. Q.; Kwong, D. L.; Wang, J. X. *Appl. Phys. Lett.* **2007**, *90*, 263501.
- Du Pasquier, A.; Chen, H. H.; Lu, Y. C. *Appl. Phys. Lett.* **2006**, *89*, 253513.
- Cheng, H. M.; Chiu, W. H.; Lee, C. H.; Tsai, S. Y.; Hsieh, W. F. *J. Phys. Chem. C* **2008**, *112*, 16359–16364.
- Chen, H. H.; Du Pasquier, A.; Saraf, G.; Zhong, J.; Lu, Y. *Semicond. Sci. Technol.* **2008**, *23*, 045004.
- Law, M.; Greene, L. E.; Johnson, J. C.; Saykally, R.; Yang, P. D. *Nat. Mater.* **2005**, *4*, 455–459.
- Feng, X.; Shankar, K.; Varghese, O. K.; Paulose, M.; Latempa, T. J.; Grimes, C. A. *Nano Lett.* **2008**, *8*, 3781–3786.
- Liu, B.; Aydil, E. S. *J. Am. Chem. Soc.* **2009**, *131*, 3985–3990.
- Mor, G. K.; Shankar, K.; Paulose, M.; Varghese, O. K.; Grimes, C. A. *Nano Lett.* **2006**, *6*, 215–218.
- Grimes, C. A. *J. Mater. Chem.* **2007**, *17*, 1451–1457.
- Zhu, K.; Neale, N. R.; Miedaner, A.; Frank, A. J. *Nano Lett.* **2007**, *7*, 69–74.
- Martinson, A. B. F.; Hamann, T. W.; Pellin, M. J.; Hupp, J. T. *Chem.—Eur. J.* **2008**, *14*, 4458–4467.
- Mora-Seró, I.; Fabregat-Santiago, F.; Denier, B.; Bisquert, J.; Tena-Zaera, R.; Elias, J.; Lévy-Clément, C. *Appl. Phys. Lett.* **2006**, *89*, 203117.
- Coleman, C. C. *Modern Physics for Semiconductor Science*; Wiley-VCH Verlag: Weinheim, Germany, 2008; p 275.
- Kuan, C. Y.; Chou, J. M.; Leu, I. C.; Hon, M. H. *J. Mater. Res.* **2008**, *23*, 1163.
- Kuan, C. Y.; Chou, J. M.; Leu, I. C.; Hon, M. H. *Electrochim. Commun.* **2007**, *9*, 2093–2097.
- Guillén, E.; Casanueva, F.; Anta, J. A.; Vega-Poot, A.; Oskam, G.; Alcántara, R.; Fernández-Lorenzo, C.; Martín-Calleja, J. *J. Photochem. Photobiol. A* **2008**, *200*, 364–370.
- Keis, K.; Lindgren, J.; Lindquist, S. E.; Hagfeldt, A. *Langmuir* **2000**, *16*, 4688–4694.
- Horiuchi, H.; Katoh, R.; Hara, K.; Yanagida, M.; Murata, S.; Arakawa, H.; Tachiya, M. *J. Phys. Chem. B* **2003**, *107*, 2570–2574.
- Greene, L. E.; Law, M.; Goldberger, J.; Kim, F.; Johnson, J. C.; Zhang, Y. F.; Saykally, R. J.; Yang, P. D. *Angew. Chem., Int. Ed.* **2003**, *42*, 3031–3034.
- Nakayama, K.; Kubo, T.; Nishikitani, Y. *Appl. Phys. Express* **2008**, *1*, 112301.
- Ito, S.; Ha, N. L. C.; Rothenberger, G.; Liska, P.; Comte, P.; Zakeeruddin, S. M.; Pechy, P.; Nazeeruddin, M. K.; Grätzel, M. *Chem. Commun.* **2006**, 4004–4006.
- Chen, C. C.; Chung, H. W.; Chen, C. H.; Lu, H. P.; Lan, C. M.; Chen, S. F.; Luo, L.; Hung, C. S.; Diau, E. W. G. *J. Phys. Chem. C* **2008**, *112*, 19151–19157.
- Xu, L.; Chen, Q.; Xu, D. *J. Phys. Chem. C* **2007**, *111*, 11560–11565.
- Peter, L. M. *J. Phys. Chem. C* **2007**, *111*, 6601–6612.
- Anderson, P. A. *Phys. Rev.* **1940**, *57*, 122–127.
- Reinaudi, L.; Del Popolo, M.; Leiva, E. *Surf. Sci.* **1997**, *372*, L309–L314.
- Wang, X. D.; Summers, C. J.; Wang, Z. L. *Appl. Phys. Lett.* **2005**, *86*, 013111.
- Sun, Z. H.; Wang, C. X.; Yang, J. X.; Zhao, B.; Lombardi, J. R. *J. Phys. Chem. C* **2008**, *112*, 6093–6098.
- Katoh, R.; Furube, A.; Barzykin, A. V.; Arakawa, H.; Tachiya, M. *Coord. Chem. Rev.* **2004**, *248*, 1195–1213.
- Kamiya, T.; Tajima, K.; Nomura, K.; Yanagi, H.; Hosono, H. *Phys. Status Solidi A* **2008**, *205*, 1929–1933.
- Benda, V.; Gower, J.; Grant, D. A. *Power Semiconductor Devices: Theory and Applications*; John Wiley & Sons Ltd.: Chichester, U.K., 1999; pp 62–65.
- Kieven, D.; Dittrich, T.; Belaidi, A.; Tornow, J.; Schwarzburg, K.; Allsop, N.; Lux-Steiner, M. *Appl. Phys. Lett.* **2008**, *92*, 153107.
- Adachi, M.; Sakamoto, M.; Jiu, J. T.; Ogata, Y.; Isoda, S. *J. Phys. Chem. B* **2006**, *110*, 13872–13880.
- He, C.; Zheng, Z.; Tang, H. L.; Zhao, L. N.; Lu, F. *J. Phys. Chem. C* **2009**, *113*, 10322–10325.
- Wu, J. J.; Chen, G. R.; Yang, H. H.; Ku, C. H.; Lai, J. Y. *Appl. Phys. Lett.* **2007**, *90*, 213109.
- Wang, Q.; Ito, S.; Gratzel, M.; Fabregat-Santiago, F.; Mora-Sero, I.; Bisquert, J.; Bessho, T.; Imai, H. *J. Phys. Chem. B* **2006**, *110*, 25210–25221.
- Dloczik, L.; Illeperuma, O.; Lauermann, I.; Peter, L. M.; Ponomarev, E. A.; Redmond, G.; Shaw, N. J.; Uhendorff, I. *J. Phys. Chem. B* **1997**, *101*, 10281–10289.
- Quintana, M.; Edvinsson, T.; Hagfeldt, A.; Boschloo, G. *J. Phys. Chem. C* **2007**, *111*, 1035–1041.
- Martinson, A. B. F.; Goes, M. S.; Fabregat-Santiago, F.; Bisquert, J.; Pellin, M. J.; Hupp, J. T. *J. Phys. Chem. A* **2009**, *113*, 4015–4021.